

EXPECTATIONS FOR INFRARED SPECTROSCOPY OF 9P/TEMPEL 1 FROM DEEP IMPACT

JESSICA M. SUNSHINE^{1,*}, MICHAEL F. A'HEARN², OLIVIER GROUSSIN²,
LUCY A. McFADDEN², KENNETH P. KLAASEN³, PETER H. SCHULTZ⁴
and CAREY M. LISSE²

¹*Science Applications International Corporation, Chantilly, VA, U.S.A.*

²*Department of Astronomy, University of Maryland, College Park, MD, U.S.A.*

³*Jet Propulsion Laboratory, California Institute of Technology, Pasadena, CA, U.S.A.*

⁴*Department of Geological Sciences, Brown University, Providence, RI, U.S.A.*

(*Author for correspondence; E-mail: sunshinej@saic.com)

(Received 23 September 2004; Accepted in final form 23 December 2004)

Abstract. The science payload on the Deep Impact mission includes a 1.05–4.8 μm infrared spectrometer with a spectral resolution ranging from $R \sim 200$ –900. The Deep Impact IR spectrometer was designed to optimize, within engineering and cost constraints, observations of the dust, gas, and nucleus of 9P/Tempel 1. The wavelength range includes absorption and emission features from ices, silicates, organics, and many gases that are known to be, or anticipated to be, present on comets. The expected data will provide measurements at previously unseen spatial resolution before, during, and after our cratering experiment at the comet 9P/Tempel 1. This article explores the unique aspects of the Deep Impact IR spectrometer experiment, presents a range of expectations for spectral data of 9P/Tempel 1, and summarizes the specific science objectives at each phase of the mission.

Keywords: coma, comets, Deep Impact, infrared spectroscopy, nucleus, Tempel 1

1. Introduction: The Importance of 1–5 μm Infrared Spectroscopy

The science payload on the Deep Impact mission includes a 1.05–4.8 μm infrared spectrometer. As described in more detail by Hampton *et al.* (2005), this spectrometer (HRI-IR) is included in the high resolution imaging system and consists of a dual prism and a 1024×512 pixel HgCdTe focal plane array (which typically is re-binned to 512×256 pixels). The HRI-IR has a minimum spectral resolution ($\lambda/d\lambda$) of ~ 200 at 2.63 μm and a maximum spectral resolution of ~ 900 at 1.05 μm . The instantaneous field of view (IFOV) is 10 μrad .

Interplanetary missions, like Deep Impact, have frequently carried near-infrared spectrometers to a wide variety of targets. The use of near-infrared spectrometers is driven by the value of this spectral region for understanding cool-to-warm bodies (vs. hot bodies, *i.e.*, stars). For objects at distances from $\sim 1/2$ to several AU from the sun, this spectral region includes the transition from reflected sunlight to thermal emission. The 1–5 μm region also includes absorption features from most ices, silicates, and organics, as well as the vibrational transitions of many compositionally

diagnostic gaseous molecules that are easily excited at the temperatures of objects at these solar distances.

The goal in designing the spectrometer is to address the key scientific objectives of the mission (A'Hearn, 2005). At the highest level, these include studying the compositional variation with depth in the nucleus and the physical process of cratering on a cometary nucleus. Since ices are the most likely component of the nucleus to show variations with depth, observations of volatiles are a necessity. In designing the Deep Impact HRI-IR spectrometer, we set a requirement for observing the fundamental vibrational transition of CO at $4.7\ \mu\text{m}$, which in turn sets the practical limit for the long-wave end of the spectral range. CO is one of the diagnostic, moderately abundant, volatiles in comets and is therefore particularly important for study. However, the product of CO abundance and the g -factor for this band is lower than for the strongest bands or blends of the other abundant volatiles. Furthermore, the fundamental vibrational band is at a wavelength at which thermal emission from the instrument itself is a problem. Taken together, this makes CO the most difficult of the abundant volatiles to observe. The IKS infrared channel of the TKS instrument on the *Vega* mission to comet Halley (Krasnopolsky *et al.*, 1986) went to a slightly longer, but quite similar long-wave limit. A sample spectrum from the IKS instrument is shown in Figure 1 (Combes *et al.*, 1988), highlighting the gaseous species producing identifiable emission features. The CO fundamental is the weakest of the clearly identified features (the OCS being a questionable detection).

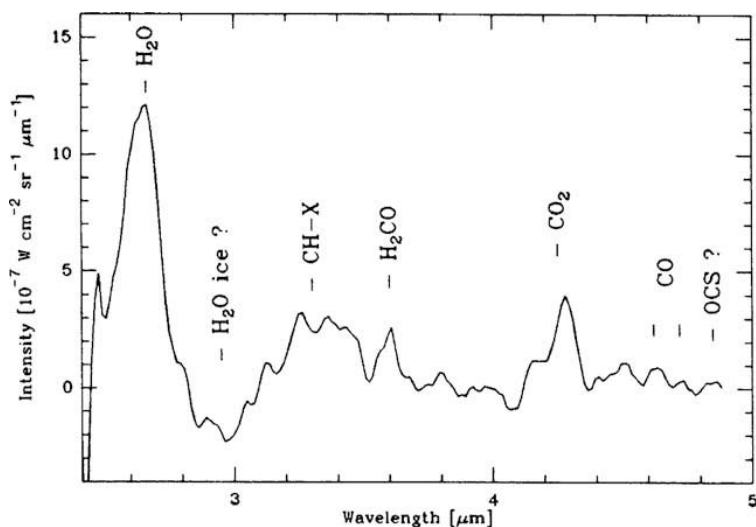


Figure 1. The *Vega* IKS spectrum of 1P/Halley 1986, taken at a distance from the nucleus of 10,000 km and at a spectral resolving power $R \sim 50$. Following Combes *et al.*, 1988, lines due to the C-H aliphatic stretch, formaldehyde, carbon monoxide and carbon dioxide are clearly present, with a possible detection of water ice absorption.

Spectroscopy of the coma *via* remote sensing is commonplace, but observations from Earth are nearly always of a very extended volume of the coma. Earth-based observations that are limited to the region near the nucleus are very rare, and are achievable only when comets approach very close to Earth. Spectra of comae include three components: (1) the solar spectrum reflected by the solid grains in comae (mostly refractory grains for remote sensing, but possibly including icy grains for observations from a close flyby), (2) thermal emission by the dust grains (which allows us to measure the superheat, or excess over the blackbody temperature, of the dust), and (3) emission-line spectra from gaseous species. If icy grains represent a significant proportion in the innermost component, as implied by models for their lifetime, then absorption features in the reflectance spectra of the dust may differ from the features in the spectra of nuclei. As with spectra of nuclei, the longer wavelengths of coma spectra will be dominated by thermal emission rather than by reflection. The exact wavelength of the break will be determined by a combination of the size distribution and the wavelength dependent indices of refraction of the individual particles. The observations from IKS (Figure 1) and observations made with a wide variety of remote sensing equipment, from ground-based telescopes through space-based telescopes like ISO, have revealed a wealth of emission features in the near-infrared.

Unlike cometary coma spectra, spectra of bare cometary nuclei are rare. An extremely limited number of telescopic spectra currently exist (e.g., Licandro *et al.*, 2002; Abell *et al.*, 2003, 2005), and only one space mission, *Deep Space-1 (DS-1)*, has ever obtained spectra of a nucleus (19P/Borrelly) without significant interference from the coma (Soderblom *et al.*, 2004b). *DS-1* dramatically documented the variation in temperature on the nucleus. The interpretation of those results will be very important in building up our understanding of the physical properties of the nucleus, particularly of the properties that influence the effective thermal inertia. However, as discussed in detail in subsequent sections, data from *DS-1* and the existing telescopic spectra indicate that on a global scale very low albedo components dominate the spectra of comet nuclei and suppress most of the plausible characteristic absorption features of common ices and silicates. While this result was important in showing that dark, presumably organic, material dominates the spectral reflectivity, it means that global spectral analysis of the nuclear reflectivity is unlikely to be diagnostic of nuclear composition. This is in contrast to objects such as icy satellites, which have significantly less dark material. Thus, for the nucleus, the ability to determine surface temperatures with good spatial resolution may be at least as important as measuring spectral absorptions.

Below, we examine in more detail previous 1–5 μm spectroscopy of cometary nuclei and comae. The Deep Impact HRI-IR spectrometer will provide measurements at previously unseen spatial resolution, before, during, and after a cratering event. We explore the unique aspects of this experiment and present a range of expectations for data of 9P/Tempel 1. Finally, we summarize the HRI-IR observation plan and highlight the specific science objectives at each phase of the mission.

2. Review of Comet Spectra from 1–5 μm

2.1. PREVIOUS RESULTS FROM OBSERVATIONS OF COMETARY NUCLEI

Our current understanding of the spectra of cometary nuclei is very limited. To date, we are aware of only five studies of the near-infrared spectral properties of bare cometary nuclei. These include four Jupiter Family comets and one Halley Family comet. Due to a new generation of instruments for telescopes and spacecraft, it is now possible to observe faint comet nuclei with reasonable signal-to-noise ratios (SNR) in the 1–2.5 μm region. However, as of yet, no spectral data on comet nuclei exist in the 2.5–5 μm region, but this region will be measured by Deep Impact's HRI-IR instrument, as described in subsequent sections.

The first published near-infrared spectra of bare nuclei were obtained by Licandro *et al.* (2002, 2003) who measured the Jupiter Family comets, 124P/Mrkos and 28P/Neujmin-1 from 0.9 to 2.3 μm using the Near-Infrared Camera Spectrometer (NICS) at the 3.56 m Telescopio Nazionale Galileo (TNG). The spectrum of 124 P/Mrkos was found to be moderately sloped, and within the signal-to-noise and spectral range, was devoid of any specific spectral features (see Figure 2). In particular, there was no evidence for water ice absorptions. These results were interpreted as probable evidence for mantling of the ice that is widely assumed to be a large component of cometary nuclei. Licandro *et al.* (2003) also note a possible

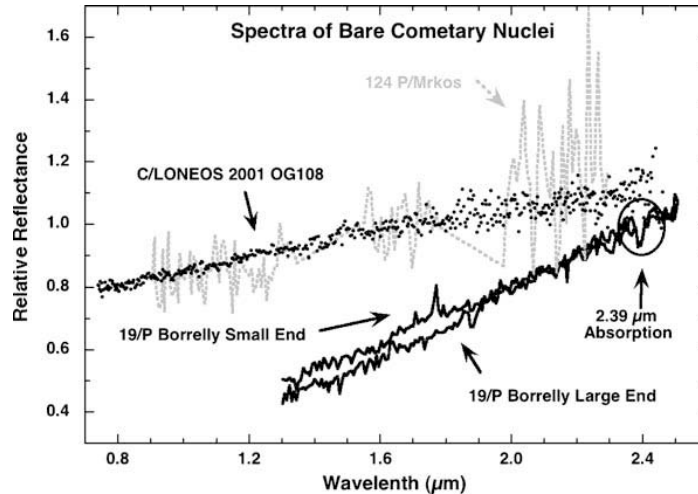


Figure 2. Existing near-infrared spectra of bare cometary nuclei. The data of 19/P Borrelly (black line) are from the *Deep Space-1* mission (Soderblom *et al.*, 2004b). Telescopic spectra of C/LONEOS 2001 OG108 (black points) are from Abell *et al.* (2003, 2005) and 124 P/Mrkos (grey dashed line) are from Licandro *et al.* (2003).

small change in slope between two nights of their observations. The NICS spectrum of 28P/Neujmin-1 is similarly featureless. However, Campins *et al.* (2003) preliminarily report significant differences in slopes between their two observations in 2001 and 2002.

The first spectrum of a bare cometary nucleus observed at the NASA Infrared Telescope Facility on Mauna Kea was measured by accident (Abell *et al.*, 2003, 2005), as part of an on-going survey of asteroids. Using the SpeX instrument (Rainer *et al.*, 2003), Abell *et al.* (2003, 2005) observed the nucleus of Halley family comet C/LONEOS OG108 at a phase angle of 8° from 0.7 to $2.5 \mu\text{m}$. At the time of observation, the object was assumed to be an asteroid, as cometary activity had yet to be observed. Even with relatively high signal-to-noise, the near-infrared spectrum of C/LONEOS OG108 was also found to have no discernible absorption features, but to be linearly increasing with wavelength, with a very similar slope to the spectrum of 124P/Mrkos (Figure 2). Based on these observations, Abell *et al.* (2003) conclude that this comet is spectrally similar to D-type asteroids.

Ground-based spectra of one other bare Jupiter family cometary nucleus have been reported. Delahodde *et al.* (2002) observed 90P/Gehrels from 1.4– $2.5 \mu\text{m}$ using the Very Large Telescope. Their preliminary comparisons suggest that there may be differences in spectral slopes and/or unspecified spectral features among their data.

Deep Space-1 (DS-1), a technology demonstration mission, provided the only space-based near-infrared spectral observations of a bare nucleus. *DS-1* encountered the Jupiter Family comet 19P/Borrelly in September of 2001 (Nelson *et al.*, 2004). Although complicated by pointing, rapidly changing Sun angles, saturation of the spectrometer signal over high albedo regions, and uncertainties in the wavelength calibration of the spectrometer, the SWIR channel of the MICAS (Miniature Integrated Camera and Spectrometer) instrument collected valuable spectra of 19P/Borrelly from 1.3– $2.5 \mu\text{m}$ (Soderblom *et al.*, 2004b). After removing instrument and thermal effects, Soderblom *et al.* (2004b) found an extremely sloped nucleus spectrum with one spectral feature at $2.39 \mu\text{m}$ (see Figure 2). In the absence of any other absorption features, specific identification of this feature has proven to be elusive. However, the absorption at $2.39 \mu\text{m}$ was present in all 46 spectra of 19 P/Borrelly and is generally consistent with organic materials, and possibly specifically with nitrogen-bearing organics. This possibility is intriguing as Kissel *et al.* (2004) report nitrogen enrichment in grains from another Jupiter family comet (81P/Wild 2) compared to grains at 1P/Halley. Although the *DS-1* spectra are much higher spatial resolution than disk averaged telescopic spectra (160 m by the width of the nucleus), there are only slight changes in spectral slope ($\sim 5\%$) from the small to the large end of the comet, as indicated on Figure 2.

Taken together these existing near-infrared observations show that on a global scale comet nuclei are spectrally featureless. Notably absent in these spectra are evidence of water ice absorptions. Instead, spectra with a variety of slopes are observed, as indicated on Figure 2. While differences in slope between comets

(and perhaps between different observations of the same comet) are clear and consistent with the range of slopes seen in visible (0.4–0.9 μm) spectra (e.g., Luu, 1993), they are not yet understood. The only example of spatially resolved data (for 19P/Borrelly) includes one absorption feature, possibly due to organics. As discussed below, even if no absorption features are present, the data from the HRI-IR spectrometer on Deep Impact, with increased spatial resolution, improved SNR, and extended spectral range, will provide new constraints on our understanding of the surface composition of comet nuclei.

2.2. PREVIOUS 1–5 μm DATA OF COMETARY COMAE

The spectra of cometary dust between 1 and 5 μm are mostly dominated by the continuum produced from the scattering of sunlight and the re-emission of absorbed sunlight as thermal radiation. The 1–5 μm continuum provides useful constraints on models of dust grain size and composition. The observed radiation depends both on the ability of the dust to scatter and emit light, and on the number of such scatterers and emitters. For dust particle mass distributions and compositions currently thought to be representative of comets (Gruen *et al.*, 1985; Lamy *et al.*, 1987; Jessberger *et al.*, 1988; McDonnell *et al.*, 1991; Lisse *et al.*, 1998), the scattered radiation (typically shortward of 3 μm) is most sensitive to the population of particles with radii $< 1 \mu\text{m}$, while the thermal emission (typically longward of 3 μm) is most sensitive to particles with radii $> 1 \mu\text{m}$. A generally decreasing slope for all comets from 0.5–3 μm has been described as being consistent with a geometrical effect in scattering from $\sim 1 \mu\text{m}$ particles (Jewitt, 1991), but Lamy *et al.* (1989) has attributed this result to compositional variations in larger grains. Variations in grain size from comet to comet suggest real differences in cometary origin and evolution. From 3–5 μm , deviations from a blackbody are very sensitive to the abundance of small, optically dark grains (Harker *et al.*, 2002; Lisse *et al.*, 2002), which can attain temperatures upwards of 600 K at 1 AU in the Sun's radiation field. Highly emissive comets like C/Hale-Bopp 1995 O1, C/Hyakutake 1996 B2, and 1P/Halley 1986 with large amounts of small particle emission have dust spectra in excess of a blackbody spectrum ("superheat"), while low activity, highly evolved comets, like 2P/Encke and 9P/Tempel 1, have dust spectra well-described by a blackbody curve.

In addition to the continuum, two specific absorption features in the 1–5 μm region have been attributed to cometary dust. A broad water ice absorption feature in the very active comet C/Hale-Bopp 1995 O1 was found by Lellouch *et al.* (1998). In addition, various authors including Combes *et al.* (1988) have discussed the possibility that the 3.2–3.5 μm emission in the VEGA-IKS spectrum of 1P/Halley (see Figure 1) is partially due to hydrocarbons in the solid phase. However, at the resolutions of the observations to date, neither of these measurements by themselves is uniquely diagnostic of the composition of the dust. The ice absorption lies on top of the liquid and gaseous water absorption and the purported 3.29 μm feature lies

among the emission lines and their associated wings from the aliphatic C-H stretch exhibited by methanol, methane, and formaldehyde.

In contrast, gas emission features in the 1–5 μm region are highly diagnostic, and most of the molecules that have thus far been detected as emissions from comets have strong fundamental vibrational bands in this region. The first breakthrough in this wavelength region was in 1986 when the *Giotto* IKS-VEGA experiment observed the spectrum of the inner coma of comet 1P/Halley between 2.4 μm and 4.9 μm , with a spectral resolution $R \sim 50$ (Combes *et al.*, 1988; see Figure 1). As predicted by Crovisier and Encrenaz (1983) using synthetic spectra, *Giotto* results clearly indicate emission lines due to H_2O at 2.7 μm , CO_2 at 4.3 μm , CO at 4.7 μm , and some unidentified CH-X molecules at 3.2–3.4 μm . H_2O was also weakly detected at 1.38 μm using the IR channel of the TKS experiment onboard the *Vega 2* spacecraft (Krasnopolsky *et al.*, 1986). The C-H stretch features, as discussed above, may be due to solid grains. Additional potential features due to H_2CO at 3.6 μm , OCS detection at 4.85 μm , and the primary absorption band due to H_2O ice at 2.9 μm are more tenuously present in the data. The CO_2 observations are particularly noteworthy, because they cannot be observed from the ground (or even high in the atmosphere from SOFIA), due to strong telluric absorptions in this region.

The second leap forward was the Infrared Space Observatory (ISO), which observed comets C/1995 O1 (Hale-Bopp) (Crovisier *et al.*, 1999a) and 103P/Hartley 2 (Colangeli, 1999; Crovisier *et al.*, 1999b) from 2.5–4.9 μm , using the spectrographs ISO/SWS with $R \sim 1500$ and PHT-S with $R \sim 90$. Emissions due to H_2O at 2.7 μm and CO_2 at 4.3 μm were detected on both comets. Emission due to CO at 4.6 μm was also detected, but only on C/1995 O1 (Hale-Bopp) (Crovisier *et al.*, 1999a). The resolution of the ISO was not sufficient to resolve the numerous emission lines possibly present in the 3.2–3.6 μm region. However, Bockelée-Morvan *et al.* (1995) analyzed spectra of seven comets observed with the IRTF and/or UKIRT with a high spectral resolution of 70–400 from 3.2–3.6 μm . They concluded that emission features in this region are mainly due to CH_3OH (methanol) fluorescence emission and probably unsaturated hydrocarbons such as PAH (Polycyclic Aromatic Hydrocarbons).

The third major advance was with the development of new instruments with very high spectral resolution $R \sim 25000$ like NIRSPEC at the Keck telescope. Using this instrument in the wavelength range 3.0–3.4 μm , Mumma *et al.* (2001) were able to identify several new emission lines. For example, on comet C/1999 H1 (Lee) they detected C_2H_6 , OH, CH_3OH , CH_4 , HCN, C_2H_2 , and NH_2 . Several emissions lines remain unidentified in the 3.3–3.5 μm region, but are most probably due to radicals or complex molecules. Finally, many molecules are known to have emission lines between 1.0 and 4.9 μm , but as of yet have only been detected at UV and radio wavelengths. One of the most interesting species is the emission of SO_2 at 4.0 μm . This feature is very weak; however, it is located in a region of the spectrum without any contamination from other emission lines. Thus while the short-lived SO_2 molecule has not yet been detected at 4.0 μm , as discussed below,

the high sensitivity and spatial resolution of Deep Impact's HRI-IR spectrometer may allow for its detection at 9P/Tempel 1.

3. Expectations for Deep Impact

Here we present what we might observe with the Deep Impact's HRI-IR spectrometer (from 1–5 μm) for the nucleus, dust, and gas coma of comet 9P/Tempel 1. Expectations are based on our current knowledge of this comet, on past IR spectroscopic observations of other comets from ground, space, and *in situ* observations, and on synthetic spectral modeling. For the first time, we will have the opportunity to observe a comet before, during, and after an impact event and at spatial scales previously unattainable. In subsequent sections, we present expectations for the nucleus pre-impact (the exterior), during the impact event, and from the post-impact crater (the interior). Similarly, we examine pre-impact expectations for the coma, from a few weeks before impact when the distance from the nucleus is several million kilometers, until a few minutes before the impact when the distance is only a few hundred kilometers. We then discuss the expectations for dust and gas emissions at the time of impact and in the subsequent minutes. Finally, we explore the range of post-impact coma phenomena that we may observe from a few minutes after impact through "look-back" observations that extend for several days.

3.1. EXPECTATIONS FOR OBSERVATIONS OF THE NUCLEUS

3.1.1. *The Pre-Impact Exterior*

The Deep Impact mission offers a unique opportunity for near-infrared observations of the surface of the nucleus of 9P/Tempel 1. As we begin to resolve the nucleus, as in the *DS-1* mission, we will obtain spectra with increasingly smaller, and ultimately negligible, coma contributions. The HRI-IR spectra will increase in resolution until a maximum of 7 m per pixel at closest approach. This represents a significant increase in spatial resolution compared to *DS-1* SWIR data of 19P/Borrelly, which had a maximum per-pixel resolution of 160 m by the width of the comet.

At these higher spatial resolutions, we expect to resolve morphologic features due to jetting and natural craters, such as those seen in the clear filter high-resolution *DS-1* images of 19P/Borrelly (Soderblom *et al.*, 2004a) and *Stardust* images of 81P/Wild 2 (Brownlee *et al.*, 2004). Differences in albedo, overall slope, and/or composition may be correlated with specific morphologies, particularly when the HRI-IR spectra are combined with 7-color visible HRI images (see Thomas *et al.*, 2005). Even in the absence of spectral features, understanding whether spectral slope varies, and if so, if it is correlated to specific processes, is of keen interest as it may help explain the variation in slopes observed in disk-integrated spectra of cometary nuclei.

The search for specific spectral features will be facilitated by a large and spatially detailed dataset that extends from 1–5 μm . The combination of increased spatial resolution, spectral range, and number of spectra available for co-adding to increase our signal-to-noise, raises the likelihood of detecting absorptions should they exist. Given the known components of cometary nuclei: silicates, organics and ices, we might observe, for example, ice-rich bright areas exposed by recent jetting or slumping that have spectral features of water, CO_2 and/or CO ice. Alternatively, we might expect dark areas, presumably rich in refractory materials, to have spectral signatures in the 1–2 μm region (due to various silicates) or in the 3.2–3.5 μm region (due to organics). We will of course examine the 2.39 μm region for the absorption band that was observed on Borrelly's nucleus (Soderblom *et al.*, 2004b) and search for additional bands at longer wavelengths that might aid to identifying its origin.

Finally, we will use the thermal signatures captured by the HRI-IR spectrometer to determine thermal variations across the nucleus. With knowledge of the rotation state (Belton *et al.*, 2005), we can relate the observed surface temperature to both the local instantaneous insolation and past history to constrain thermal inertia.

3.1.2. *The Impact Event*

The Deep Impact collision may produce a significant 'flash'. Observations of hypervelocity impacts into a wide range of material types (Ernst and Schultz, 2003, 2004; Schultz and Ernst, 2005) reveal that the luminous efficiency (radiant energy scaled to initial impact kinetic energy) may range from 10^{-5} – 10^{-3} and will depend on the nature of the upper surface of the comet. Laboratory experiments impacting silicate targets with velocities from 5–6 km/s resulted in peak temperatures exceeding 6000 K that rapidly decayed to temperatures of around 2800 K to 3200 K over more than 1 millisecond. This thermal evolution results from ejecta that includes heated silicate particles and melt droplets that line the crater floor. Integrating the total energy over time and wavelength yielded a cumulative radiant energy of about 0.7 joules, which represents about 0.035% of the initial kinetic energy. The radiation is a thermal component related to heated particulates from the target. As described in more detail by Schultz and Ernst (2005), the cumulative radiant energy can be scaled to the Deep Impact collision over the 1–5 μm range of the HRI-IR, which yields an integrated radiant energy of 5 mega-joules in about 100 milliseconds. However, the total duration of the impact flash may be as long as 500 milliseconds to 1 s, depending on composition. Thus, as detailed in Schultz and Ernst (2005), this observation, may provide an estimate of the silicate-to-volatile ratio of 9P/Tempel 1.

The spatial field-of-view of the HRI-IR spectrometer slit allows for tracking of the evolution of different ejecta components through time. Time-exposed spectra (seconds) of vapor plumes from hypervelocity impacts in the laboratory (lasting less than 50 microseconds) illustrate the successful application of this strategy, as long as there is sufficient radiant flux (Schultz, 1996). As the imaged plume passed

the slit, evolving spectra were successfully recorded. For the Deep Impact HRI-IR spectrometer, the projected slit width at the time of impact will be 85 m, while the slit length will extend across ~ 5.4 km of the comet surface (Klaasen *et al.*, 2005). The first several spectra after impact should capture the vapor phases and thermal components. Rapid expansion of the plume should then smear the source at certain locations in the slit during the exposure.

For Deep Impact, the horizontal velocity component of the initial plume (combined with its optical depth) will control the observed spectra. Even though the initial plume expansion velocities may exceed 10 km/s, most of the early stages will have significantly lower velocities. If the near surface of the comet is highly porous, vapor phases developed within the cavity initially will be directed upwards (toward the Deep Impact spacecraft), thereby reducing lateral growth (e.g., see Schultz and Ernst, 2005). In this case, much of the earliest evolution of the plume could be captured within the HRI-IR slit with an intensity limited by the optical depth of the ionized gases. If the upper surface layers (depth of ~ 1 – 5 m) have significant strength, then it is likely that the HRI-IR will capture radiating components in streaks. Although not time resolved, the spatially restricted radiating sources will be captured.

It is expected that the vapor plume will then evolve with time (next several seconds) due to changing temperatures and chemical reactions. However, subsequent spectra will record cooler ejecta from depth, including primary volatile species. This component will emerge closest to the observation point as the higher temperature constituents move toward either end of the slit. Solar fluorescence may then reveal primary atomic and molecular species of interest. Even though the radiating phases may have left the region of impact, their contribution to the spectra may persist depending on the horizontal component of the velocity. If the surface is composed of silicates, these spectra also will exhibit a strong thermal background and provide a direct measure of the temperature, which will be useful to characterize the nature of the surface (see Schultz and Ernst, 2005).

During the subsequent ~ 300 – 800 s after crater formation, ejecta from the nucleus will pass over the HRI-IR spectrometer slit. Over time, these ejecta will originate from greater and greater depths, and will be spatially separated along the slit. As such, observing ejecta as a function of time will provide data on composition as a function of depth in the nucleus. Our expectation is to first see refractory materials coming from the surface (organics and silicates), followed by an increase in volatile species (e.g., H_2O , CO , CO_2), which will likely include some ices. Over this time period, the temperature of ejecta will vary due to competing effects of the energy released by the impact and the intrinsic temperature profile of the nucleus, which arise from changes in solar insolation and thermal inertia.

3.1.3. *The Post-Impact Crater Floor*

After the crater formation event, and with some luck in our pointing, the HRI-IR spectrometer will be able to observe the interior of our newly created crater and

its surrounding ejecta deposits. This unique observation, will for the first time, measure the exposed interior of a comet nucleus. If the surfaces of comet nuclei are covered by a mantling process (ionic space weathering or residual buildup of refractory materials) as is commonly thought (e.g., Brin and Mendis, 1979; Johnson *et al.*, 1987), then the Deep Impact crater should reveal more pristine materials. The candidate materials for near-surface comet interiors include ices (water, CO₂, methane, etc.), silicates, and various organic materials.

The HRI-IR spectrometer is well suited to detect these materials should they exist. The primary silicates, olivine and pyroxene, if they include even minor amounts of iron, have diagnostic absorptions in the 1 and 2 μm regions due to electronic transitions of Fe²⁺ ions in crystallographic sites within the silicate structures (Burns, 1993). Spectra of related hydrated silicates include overtones and combinations of overtones of vibrational, bending, and stretching bands of bound H₂O and OH- ions in the 1.4–2.4 μm region (Hunt, 1979; Hunt and Ashley, 1979). Planetary ices have several vibrational and overtone features in the near-infrared, which can vary with temperature and grain size (e.g., Clark, 1981). Major absorptions include: water ice at 1.25, 1.6, 2.0, 2.9, and 3.1 μm ; methane ice at 1.7, 2.3, 2.6, and 3.3 μm ; methanol ice at 2.27 μm ; CO ice at 1.6, 2.3, and 4.7 μm ; CO₂ ice at 2.0, 2.7, 3.3, and 4.3 μm , and ammonia ice at 1.5, 1.6, 2.0, 2.3, and 2.9 μm (e.g., Coradini *et al.*, 1998; Quirico *et al.*, 1999). Spectra of natural organics contain C-, H-, and O-vibrational modes that also lead to a variety of features in the 1.5–3.5 μm region (e.g., Cloutis, 1990; Moroz *et al.*, 1998).

While few comet exteriors and no comet interiors have been observed in the near-infrared, a number (although still relatively few) observations of Trans-Neptunian objects (TNOs), (*i.e.*, Kuiper Belt Objects or Edgeworth-Kuiper Belt Objects) have been made (e.g., Barucci *et al.*, 2005). The TNO's and Centaurs, a population derived from TNO's by perturbations with Neptune (Barucci *et al.*, 2002), are now widely accepted as the source region for short period comets (e.g., Levison and Duncan, 2001). As such, the composition of TNO's is highly relevant to the study of comets. The spectra of a number of TNO's include absorptions from a variety of the possible cometary nucleus materials, suggesting that if these materials are present and not masked by darkening agents, they should be detectable at 9P/Tempel 1 with the HRI-IR spectrometer.

Due to their faintness, very few near-infrared spectra of TNO objects exist. As recently summarized by Barucci *et al.* (2005), the signal-to-noise of these spectra are low, but those observed are diverse and suggest non-uniformities on the surfaces of some TNO's. Some are generally flat, yet featureless (e.g., 1996 TL66; Luu and Jewitt, 1998) while others show strong water ice absorptions (e.g., 19308/1996 TO66; Brown *et al.*, 1999, 2000; Licandro *et al.*, 2001). The spectra of one object 26375/1999 DE9 includes absorptions near 1.4, 1.6, 2.0, and 2.25 μm attributed to hydrous silicates and possibly a 1 μm olivine feature (Jewitt and Luu, 2001).

The spectra of Centaurs, as summarized by (Barucci *et al.*, 2002, 2005), are dominated by water ice absorptions. While featureless in the visible, the near-infrared

spectrum of 2060 Chiron (Luu *et al.*, 2000) includes water ice features in the 1.5 and 2 μm regions, as does 10199 Chariklo (Brown and Koresko, 1998; Dotto *et al.*, 2003). Recent modeling by Groussin *et al.* (2004a) indicates that both Chiron and Chariklo contain 70–80% non-ice materials (silicates, carbon, or kerogen). 8405 Asbolus, while globally featureless in Earth-based spectra (Brown, 2000; Barucci *et al.*, 2000), showed strong water absorption in Hubble Space Telescope observations (Kern *et al.*, 2000).

Among all solar system objects, the Centaur 5145 Pholus stands out based on its extremely sloped near-infrared spectrum with absorptions at 2.04 and 2.27 μm , assigned to water ice and methanol ice, respectively (Cruikshank *et al.*, 1998). Cruikshank *et al.*'s radiative transfer modeling suggests a significant component of olivine, amorphous carbon (a darkening agent), and moderate amounts of organics (tholins). Taken together the existing spectra of TNO's and the derivative Centaurs suggest the range of spectral features that might be observable in the interior of 9P/Tempel 1. Deep Impact's HRI-IR, with extended coverage out to 5 μm , may reveal more features that might aid in identifying specific materials.

Remote observations of TNO's are, of course, of their exterior surfaces. The surfaces of TNO's are thought to be subject to a variety of processes that affect their spectral properties and in particular may explain their color diversity (Barucci *et al.*, 2005). Exposure to solar radiation, solar, galactic, and cosmic-ray irradiation, or space weathering, will produce slopes that increase toward longer wavelengths. In contrast, the collision-resurfacing hypothesis (Luu and Jewitt, 1996), suggests that more neutrally sloped spectra could be restored by regular resurfacing from mutual collisions. Recent work by Moroz *et al.* (2004) suggests that the spectra of organics may also become neutral when exposed to space weathering. Finally, sporadic cometary activity, for those objects closer to the sun (the Plutinos), may result in resurfacing by re-condensed ice (Hainaut *et al.*, 2000).

These same processes, in different relative proportions and acting over much different time scales, are likely to be present on comet nuclei. As we compare the interior of 9P/Tempel 1 to observations of its exterior, the Deep Impact experiment will help us understand these processes, at least for short period comets; the smallest, warmest, and youngest members of the TNO family. In addition, our inferences about the interior of 9P/Tempel 1 are likely to reveal a higher volatile content than inferred from observations of the nucleus exterior. These data may therefore provide a more useful comparison to the surfaces of TNO's, which have yet to be significantly devolatilized by heating in the inner solar system.

3.2. EXPECTATIONS FOR OBSERVATIONS OF THE COMA

3.2.1. *Pre-Impact*

Comet 9P/Tempel 1 is a typical Jupiter family comet with a Tisserand parameter of 2.97 and an orbital period of 5.5 years. Combining the Spitzer infrared

and HST visible observations from March 2004, HST visible observations from May 2004, and several H₂O production rates measured during the 1994 passage (A'Hearn *et al.*, 1995; Fink *et al.*, private communication), Groussin *et al.* (2004b) derived a nucleus mean radius of 3.3 ± 0.2 km, a visible geometric albedo of 0.04 ± 0.01 , and an active fraction of $8.3 \pm 2.2\%$ for 9P/Tempel 1 (see Belton *et al.*, 2005). With an 8% active fraction, 9P/Tempel 1 is a low activity comet compared to other Jupiter family comets like 22P/Kopff (35% active fraction; Lamy *et al.*, 2002), 103P/Hartley2 (100% active fraction; Groussin *et al.*, 2004c), or 46P/Wirtanen (85% active fraction; Groussin and Lamy 2003). Visible observations using narrow band filters (A'Hearn *et al.*, 1995) and UV spectroscopic observations (Fink *et al.*, private communication) allowed the detection of several coma species with relative abundances typical of Jupiter family comets. These include: OH (1.1×10^{28} molecules/s at perihelion), CN ($\log \text{CN/OH} = -2.8$), C₂ ($\log \text{C}_2/\text{OH} = -2.9$), C₃ ($\log \text{C}_3/\text{OH} = -4.1$), NH ($\log \text{NH/OH} = -2.6$), and NH₂ ($\log \text{NH}_2/\text{OH} = -2.8$). A more detailed discussion of the dust and gas coma of 9P/Tempel 1, is presented in a companion paper by Lisse *et al.* (2005).

The only spectrum of a Jupiter family comet coma currently available at high-enough resolution to identify the numerous gaseous species in the 1–5 μm range is of 103P/Hartley 2 obtained with the ISOPHOT-S instrument (Colangeli, 1999). This comet is smaller than 9P/Tempel 1 with a radius of 0.71 km (Groussin *et al.*, 2004c), but has a similar H₂O production rate of 1.2×10^{28} molecules/s at perihelion (Crovisier *et al.*, 1999b), which allows for useful comparisons. Based on their presence in the spectrum of 103P/Hartley 2, we should be able to detect the emission lines of H₂O at 2.7 μm and CO₂ at 4.3 μm in the coma of 9P/Tempel 1.

The unique Deep Impact experiment will allow us to collect data at a higher spectral resolution than ISO ($R \sim 200\text{--}900$ vs. $R \sim 90$), a larger wavelength range (1–5 μm vs. 2.5–5.0 μm), and the highest spatial resolution ever obtained (only 7 m per pixel at closest approach). Taking advantage of the larger wavelength range, we should detect the weak emission lines of H₂O at 1.4 μm and 1.9 μm . The high spectral resolution will allow us to resolve the two peaks of CO emission at 4.7 μm (if it is present) and some emission lines in the 3.1–3.6 μm region. In particular, we expect to see broad CH₃OH emission lines at 3.4 μm and H₂CO at 3.6 μm .

The very high spatial resolution will also allow us, for the first time, to differentiate between jets and non-jet regions, providing an opportunity for direct spectral comparisons. Jets have already been observed on 9P/Tempel 1 (Lisse *et al.*, 2005; Biver, private communication) and we expect to see differences in the absolute and relative composition between jets and non-jet regions. In particular, we expect more highly volatile species in the jets (e.g., CO and CO₂). As Deep Impact approaches the nucleus, the spatial resolution will increase and we will be able to explore the near nucleus coma, which is not resolvable from the ground. If they exist in enough quantity, this may allow for the detection of species with relatively short lifetime such as SO₂ at 4.0 μm or NH₃ at 2.3 μm . Both SO₂ and NH₃ have very

weak emission lines but are located in a very clear region of the spectrum, which facilitates their detection.

In order to improve our predictions and illustrate the capacities of the Deep Impact HRI-IR spectrometer, we developed a preliminary model to calculate synthetic spectra of 9P/Tempel 1 as they may appear during the mission. A similar analysis was performed on the VIRTIS instrument on *Rosetta* (Coradini *et al.*, 1998). Our model is adapted from the formalism of Crovisier and Encrenaz (1983). Taking into account resonance fluorescence for the gas emission and a Haser's model for the gas density, we selected the most abundant species in comets for which molecular band position, intensity, and shape are known. These species are given in bold in Table I. For each species we selected the fundamental and combination bands located in the 1–5 μm region and their line intensities from the HITRAN database, except for CH_3OH which is adapted from Bockelée-Morvan *et al.* (1995). For the combination bands, we assume an emission rate equal to the excitation rate, *i.e.* we do not take into account the de-excitation of combination bands through intermediate levels (hot bands). This assumption leads to an over-estimate of the flux from combination bands like H_2O at 1.38 μm and 1.88 μm , and OCS at 2.44 μm and 4.0 μm . The dust continuum is modeled with a density proportional to $1/r^2$ (where r is the distance from the nucleus) and a size distribution function for the grains with a relative slope of -3.7 , a minimum grain size of 0.1 μm , and a maximum grain size of 1 cm (Lisse *et al.*, 1998). For the nucleus continuum, the visible light is reflected on the nucleus assuming a Lambertian surface with a Bond albedo of 0.03 and the thermal emission is calculated assuming a constant surface temperature of 320 K (upper limit). Initial compositions are set to those of C/1995 O1 Hale-Bopp, for which we have the largest dataset of detected species (see Table I). The model includes many parameters that can then be modified including composition, distance to the nucleus, gas velocity, nucleus temperature, grain escape velocity, etc. . . . We chose a reasonable set of parameters, given in Table II, to support our goal of investigating likely scenarios for the Deep Impact spectrometer.

Figures 3 and 4 illustrate the results for two modeled spectra with a slit on the nucleus calculated 10 days and 1 day before impact, respectively. In both cases, the signal is strongly dominated by the nucleus continuum and very few emission lines are visible. At 10 days out (Figure 3) some coma emissions of H_2O at 1.4, 1.9 and 2.7 μm and CO_2 at 4.3 μm are detectable (but CO_2 is very weak). However, 1 day before impact (Figure 4) the nucleus so dominates that only H_2O at 2.7 μm is observed. These results indicate that for maximum scientific return on the coma a few days before impact, we must observe the coma away from the nucleus in order to increase the S/N ratio.

Such an observation is illustrated by Figure 5, which shows a modeled spectrum 1 day before impact with a slit ~ 90 km off the nucleus. In the absence of the nucleus, we can identify several species. The main emission lines are due to H_2O at 1.4, 1.9, and 2.7 μm , CH_3OH at 3.4 μm , H_2CO at 3.6 μm , CO_2 at 4.3 μm , and CO at 4.7 μm (double peaks). We also see weaker emission lines of NH_3 at 2.3 μm and

TABLE I

A non-exhaustive list of emission lines of molecules detected in comets (many of which have yet to be detected in the 1–5 μm region).

Molecule ^a	Wave number (cm^{-1})	Wavelength (μm)	X/H ₂ O for Hale-Bopp
HCO	9297	1.08	–
CN	9117	1.10	–
N ₂ ⁺	9016	1.11	–
C ₂	8268	1.21	–
H₂O	7250	1.38	1
C ₂	6928	1.44	–
C ₃	6482	1.54	–
C ₂	5633	1.78	–
H₂O	5331	1.88	1
NH₃	5070	1.97	0.007
NH₃	4400	2.27	0.007
CH₄	4340	2.30	0.006
C ₂ H	4106	2.44	–
OCS	4101	2.44	0.004
C ₂ H	4011	2.49	–
H₂S	3846	2.60	0.015
C ₂ H	3785	2.64	–
C ₂ H	3773	2.65	–
H₂O	3756	2.66	1
CO₂	3715	2.69	0.06
HDO	3707	2.70	–
C ₂ H	3692	2.71	–
CH₃OH	3681	2.71	0.024
HNC	3653	2.74	–
CO₂	3612	2.77	0.06
OH	3568	2.80	0
HNCO	3538	2.83	–
H ₃ O ⁺	3530	2.83	–
H ₃ O ⁺	3514	2.85	–
NH₃	3333	3.00	0.007
HCN	3311	3.02	0.0025
NH ₂	3301	3.03	–
C₂H₂	3295	3.03	0.001
C₂H₂	3282	3.05	0.001
H ₂ O ⁺	3259	3.07	–
NH ₂	3219	3.11	–

(Continued on next page)

TABLE I
(Continued)

Molecule ^a	Wave number (cm ⁻¹)	Wavelength (μ m)	X/H ₂ O for Hale-Bopp
H ₂ O+	3213	3.11	–
NH	3127	3.20	–
HCO+	3089	3.24	–
HCOOCH ₃	3045	3.28	–
H ₂ CS	3025	3.31	–
CH₄	3019	3.31	0.006
CH ₃ CN	3009	3.32	–
CH₃OH	2999	3.33	0.024
C₂H₆	2985	3.35	0.003
H ₂ CS	2971	3.37	–
CH₃OH	2970	3.37	0.024
HCOOCH ₃	2969	3.37	–
OH+	2956	3.38	–
CH ₃ CN	2954	3.39	–
HCOOCH ₃	2943	3.40	–
OCS	2918	3.43	–
CH₃OH	2844	3.52	0.024
H₂CO	2843	3.52	0.011
HC ₃ N	3327	3.55	–
H₂CO	2782	3.59	0.011
CH+	2754	3.63	–
CH	2733	3.66	–
HDO	2727	3.67	–
H₂CO	2719	3.68	0.011
SO₂	2500	4.00	0.0023
CO₂	2349	4.26	0.06
CO₂	2337	4.28	0.06
HC ₃ N	2272	4.40	–
HNCO	2269	4.41	–
CH ₃ CN	2268	4.41	–
CO+	2184	4.58	–
HCO+	2184	4.58	–
CO	2143	4.67	0.23
OCS	2062	4.85	0.004

^aFor most of these molecules, the shape and/or the intensity of the emission lines are unknown and we cannot include them in our model (e.g., Figure 6). Only the most abundant species (indicated in bold) are currently included in the model. Data are taken from HITRAN (Rothman *et al.*, 2003) and Crovisier's databases (<http://www.usr.obspm.fr/~crovisie/basemole/>), and from Bockelée-Morvan *et al.* (1995) for CH₃OH. The X/H₂O production rate ratios for C/1995 O1 Hale-Bopp come from Bockelée-Morvan *et al.* (2000).

TABLE II

A list of the model parameters used to generate the synthetic HRI-IR spectra.

Spacecraft /comet distance	8.8×10^9 m 10 days before impact 8.8×10^8 m 1 day before/after impact
Comet/Sun distance (at time of impact)	2.25×10^{11} m
Phase angle (at time of impact)	63°
Nucleus radius	3.4 km
Nucleus Bond albedo	0.03
Nucleus IR emissivity	0.95
Nucleus sub-solar temperature	320 K
Minimum size of dust grains in the coma	1.0×10^{-7} m
Maximum size of dust grains in the coma	0.01 m
Slope of the dust grains differential size distribution	-3.7
Dust grain Bond albedo	0.08
Dust grain IR emissivity	0.92
Dust grain temperature	245 K
Dust grain expansion velocity	300 m/s
Dust grain density	2500 kg/m^3
Gas expansion velocity	1000 m/s
Gas temperature	296 K (HITRAN database)
Dust to gas ratio	1 before impact, 3 after impact
Water production rate (at time of impact)	1.0×10^{28} molecules/s
Composition relatively to water	Similar to Hale-Bopp ^a

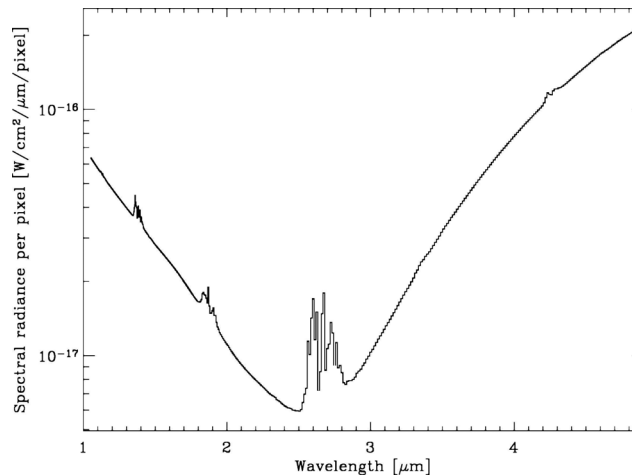
^aSee Table I.

Figure 3. Modeled spectrum of comet 9P/Tempel 1 as seen with the Deep Impact HRI-IR spectrometer 10 days before impact with the slit on the nucleus. Emission lines from H₂O at 1.4, 1.9 and 2.7 μm are clearly visible. Emission lines from CO₂ at 4.3 μm are extremely weak.

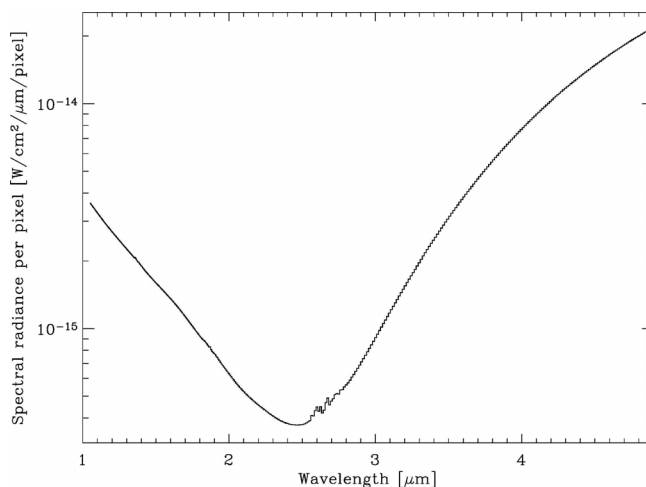


Figure 4. Synthetic spectrum of comet 9P/Tempel 1 as seen with the Deep Impact HRI-IR spectrometer, 1 day before impact with the slit on the nucleus. Only emission lines from H₂O at 2.7 μm are visible.

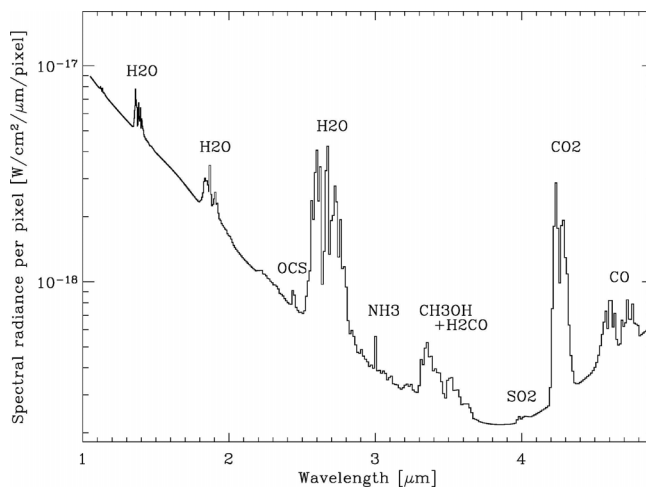


Figure 5. Synthetic spectrum of comet 9P/Tempel 1 as seen with the Deep Impact HRI-IR spectrometer 1 day before impact with a slit ~ 90 km off the nucleus. Emission lines from H₂O at 1.4, 1.9 and 2.7 μm, CH₃OH at 3.4 μm, H₂CO at 3.6 μm, CO₂ at 4.3 μm, the two peaks of CO at 4.7 μm, NH₃ at 3.0 μm, and OCS at 2.44 μm are clearly visible. SO₂ at 4.0 μm is weakly visible. Note that for illustrative purposes, the ratio NH₃/H₂O, OCS/H₂O and SO₂/H₂O were artificially increased by a factor of 20 (compared to C/1995 O1 Hale-Bopp). As described in the text, we do not think their actual detection at 9P/Tempel 1 is very probable.

3.0 μm , OCS at 2.44 μm , and broad emission lines of SO_2 at 4.0 μm . However, it is important to note that for illustrative purposes we have increased the ratio of $\text{NH}_3/\text{H}_2\text{O}$, $\text{OCS}/\text{H}_2\text{O}$ and $\text{SO}_2/\text{H}_2\text{O}$ by a factor of 20, compared to C/1995 O1 Hale-Bopp (see Table I). For 9P/Tempel 1, we expect ratios similar to those of C/1995 O1 Hale-Bopp or lower, and thus detection of NH_3 , OCH, and SO_2 , will in fact be very challenging and improbable.

As discussed above, most information on dust will come from the analysis of the dust continuum. The best regions to estimate this continuum are in the spectral regions that are free from emission lines. As indicated on Figure 3, such regions include 1.2–1.3 μm , 1.5–1.8 μm , 2.0–2.2 μm , and 3.7–3.9 μm . Modeling reflected light from dust grains and their thermal emission allows us to fit the observed continuum and derive some physical properties of the grains, such as their temperature and size distribution function (Lisse *et al.*, 1998). However, the solution is often non-unique and the derived properties are usually model dependent. Prior to impact, we will carry out many observations at different distances from the nucleus and at different positions in the coma, from which we expect to solve the model ambiguities and build a globally consistent overview of the dust properties (mainly temperature and size distribution). As with gas emissions, one of Deep Impact's most unique dust measurements will be to take advantage of our very high spatial resolution to compare the dust in jets and non-jet regions. More details on dust observations with Deep Impact can be found in Lisse *et al.* (2005).

3.2.2. Impact Event

The impact event should lift off a significant amount of dust particles from the surface and interior of the nucleus. Large grains that usually cannot lift off from the nucleus by gas sublimation and drag forces alone will escape the nucleus because of the impact energy. We expect to see significant changes in the dust continuum at the time of impact. In particular, the impact will produce ejecta at high temperature that will strongly increase the thermal component of dust continuum in the 3–5 μm region. Subsequent cooling rates will depend on grain size, thermal conductivity, density, and composition, which may be determined from studying the temporal variations of the dust continuum after impact. In addition, from our observations we should be able to estimate the maximum size of a grain that can be ejected from the nucleus, a very important constraint on activity models (*e.g.*, Groussin and Lamy, 2003). At the same time, if the reflected component of the dust continuum increases strongly, it will reveal the presence of numerous micron and sub-micron size particles on the surface and interior of the nucleus, indicating the presence of very friable refractory materials, a low cohesion force between the grains, and/or very low grain density.

The chemistry of gases at the time of impact will be difficult to sort out. Over the short-term, the physics is quite complex. With excess heat and the presence of exotic materials, a wide range of species may be produced. During the late stages of excavation, however, relatively unaltered materials from the nucleus should be

added to the coma. Over a longer time scale (see below), we expect to monitor the increased thermal signature and potentially detect changes in emission ratios and even new emission features.

3.2.3. *Post-Impact*

The major objective for post-impact spectroscopic observations of the coma is to monitor activity and look for any changes in the gas and dust coma after impact. As discussed above, the determination of the physical properties and composition of the coma is model dependant, and many observations before, during, and after the impact are necessary to better constrain the models and reduce their uncertainties.

For the gas coma, we expect the impact to reveal fresh volatile materials, which will cause increases in the production rates and will likely significantly change the relative abundances of different molecules. The highly volatile species (CO and CO₂) are expected to be located under the surface where they are protected from direct insolation. As such, the impact should produce an increase in CO and CO₂ relative to water. While it is impossible to quantitatively predict this enrichment, a factor of 10–100 relative to water is possible. This enrichment will be stronger in the jets resulting from impact (if they exist) than in the other region of the coma. Figure 6 illustrates what a spectrum would look like 1 day after impact with a slit ~ 90 km off the nucleus, assuming an enrichment of all species (except CH₃OH, see below) relative to water by a factor 20 compared to C/1995 O1 Hale-Bopp. We have

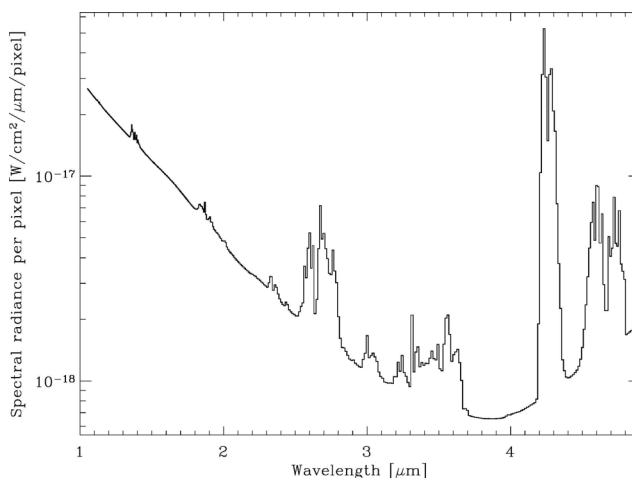


Figure 6. Synthetic spectrum of comet 9P/Tempel 1 as seen with the Deep Impact HRI-IR spectrometer, 1 day after impact with a slit ~ 90 km off the nucleus. Emission lines from H₂O at 1.4, 1.9 and 2.7 μm , CH₃OH at 3.4 μm , H₂CO at 3.6 μm , CO₂ at 4.3 μm , CO at 4.7 μm (double peak), NH₃ at 2.2–2.3 μm , OCS at 2.44 μm , HCN at 3.0 μm , and CH₄ at 3.31 μm are identified. As discussed in the text, the ratio of all molecules (except CH₃OH) were increased by a factor of 20 relative to water, while the dust to gas ratio was increased by a factor of 3 relative to pre-impact values.

also increased the dust-to-gas ratio by a factor of 3 relative to pre-impact values, to represent the larger amount of dust in the coma after impact. A comparison with Figure 5, which represents the same observational conditions before impact, indicates that SO_2 at $4.0 \mu\text{m}$ is no longer visible, due to the increase of a factor of 3 of the dust continuum. However, we are now able to detect new species such as HCN at $3.00\text{--}3.05 \mu\text{m}$ and CH_4 at $3.31 \mu\text{m}$. The detection of CH_4 will only be possible if CH_3OH does not increase during impact, otherwise the CH_3OH emission dominates the $3.2\text{--}3.6 \mu\text{m}$ region and masks the detection of other species with weaker emission lines. With a spectral resolution $R \sim 200$, the interpretation of features from $3.0\text{--}3.6 \mu\text{m}$, a region very rich in emission lines, is expected to be difficult.

After impact, molecules never before identified in the $1\text{--}5 \mu\text{m}$ region may appear in the coma. Table I presents a non-exhaustive list of molecules identified in comets that have emission lines in the infrared region, many of which have yet to be detected in the infrared. For most of these molecules, the shape and the intensity of the emission lines are unknown, and we therefore cannot include them in our model (e.g., Figure 6). Only the most abundant species are currently included in the model (in bold in Table I). The large number of molecules, more than 40, illustrates the wealth of potential in the $1\text{--}5 \mu\text{m}$ region. However, this also presents an interpretive challenge with several emission lines likely to overlap, suggesting the complexity awaiting our analysis, as the model solutions are unlikely to be unique. It is also possible that Deep Impact will detect emission lines not listed in Table I, leading to the identification of a new molecule in comas. Finally, if no changes in the gas coma are observed after impact, it would call into question our current model of cometary nuclei.

For the dust, we expect to see significant changes in the reflected and thermal continuum, which will allow us to better constrain the physical properties of the grains. As the properties of the dust are currently poorly known, it is very difficult to make predictions on what we will actually observe. However, the impact should increase the dust production rate, rapidly increase the temperature (which will then decrease post-impact), and modify the size distribution of the grains. All these phenomena should be observable by studying the dust continuum post-impact at different times and positions in the coma. Determining if the impact has a global effect on the coma or just a localized effect near the impact region, is of particular interest. As with the gas coma, observing no changes in the dust after impact would be very surprising, yet very interesting, and would also oblige us to completely review our current view of comets.

4. Summary

A comprehensive set of nucleus and coma observations using the HRI-IR spectrometer is planned for Deep Impact, before, during, and after the impact event to support the science described above. The measurements to be made will allow a number

of important experiments to be conducted at 9P/Tempel 1. Most of the planned observations will provide information for multiple spectroscopy objectives, since the spectrometer slit often includes both the nucleus and the nearby coma at the same time. The spectroscopy science goals can be broadly categorized as:

- Variations in coma and the disk-integrated nucleus spectrum versus rotation phase
- Pre-impact coma composition, structure, and evolution at high spatial resolution
- Disk-resolved nucleus composition and temperature over one hemisphere
- Thermal profile of the impact event
- Impact ejecta composition (both gas and dust) versus time from impact
- Composition of the interior of the nucleus as exposed by the crater and its ejecta deposits
- Post-impact coma composition, structure, and evolution

Table III summarizes the planned HRI-IR spectrometer observations and the science goals that are expected to be addressed with each observation. A more detailed discussion (with additional measurement specifics) of the anticipated HRI-IR spectrometer data set is given in the companion paper by Klaasen *et al.* (2005).

A typical exposure time of 2.88s, yields the predicted mean signal levels in instrument data number (DN) units and the SNRs listed in Table IV for spatially resolved nucleus and coma scenes. For this calculation, the nucleus is assumed to have an albedo 5% and phase coefficient at 63° of .047. As described in Hampton *et al.* (2005), the central third of the HRI-IR spectrometer includes an anti-saturation filter, designed to block thermal contributions above 3.5 μm when observing the nucleus. SNRs at the longer wavelengths are given both for a 200 K surface outside the anti-saturation filter (which covers the central 1/3 of the spectrometer slit) and for a 300 K surface behind the anti-saturation filter. A 300 K surface outside the filter will be saturated. The predicted coma SNRs are highly uncertain; the numbers in Table IV assume that the coma is 20 times dimmer than the nucleus and has the same spectrum. In these calculations, the coma is assumed to be no warmer than 200 K. Coma SNRs can be increased at the expense of spatial resolution by averaging over spatial blocks of pixels during post-processing. Nucleus SNRs can similarly be boosted, by spectral summing, particularly over the 1.0–2.5 μm range, which covers the first half of the focal plane array. Predicted mean DN levels scale linearly with exposure time. SNR scales approximately linearly with exposure at low signal levels (<50 DN) and approximately as the square root of exposure at high signal levels (>200 DN).

The Deep Impact IR spectrometer was designed to optimize, within engineering and cost constraints, observations of the dust, gas, and nucleus of 9P/Tempel 1. The wavelength range of 1–5 μm includes absorption and emission features from ices, silicates, organics, and many gases that are known to, or expected to be, present on comets. Deep Impact is a unique experiment in that it will allow us to observe the

TABLE III

A summary of the Deep Impact HRI-IR spectrometer observation plan at each mission phase.

Time ^a	Pixel Scale (m)	Scientific goals	Data description	Comments
Far Approach				
I-60 d to I-25 h	>9,000	Rotation Pre-impact coma	Spatial scans with longer exposures every 4 h	Includes a full resolution scan of extended coma
I-25 h to I-11 h	>4,000	Rotation Pre-impact coma nucleus	Spatial scans every 2 h	
I-10 h		Calibration	Dark levels all instrument modes	Last pre-impact calibration
Approach				
I-9 h to I-1 h	>400	Pre-impact coma nucleus	Spatial scans	Includes full resolution scan of inner coma at I-1 h
I-36 m to I-19 m	>200	Pre-impact coma nucleus	Full nucleus scans	
I-14 m to I-10 m	>145	Pre-impact coma nucleus	Partial coma scan	3 full resolution at edges and nucleus center
I-6 m to I-66 s	>95	Pre-impact coma	Full nucleus scans	Last pre-impact scan
I-35 s to I-9 s	87	Pre-impact coma nucleus	Exposures every 2.88 s	
Impact				
I-6 s to I+15 s	85	Impact thermal signature ejecta monitoring	Very short exposures every 0.72 s	
I+15 s to I+32 s	83	Ejecta monitoring	Short exposures every 1.44 s	
I+32 s to I+50 s	81	Ejecta monitoring	Exposures every 2.88 s	
I+50 s to I+67 s	79	Ejecta monitoring nucleus interior	Crater scan	
I+70 s to I+78 s	78	Ejecta monitoring post-impact coma	3 exposures	
I+87 s to I+107 s	76	Ejecta monitoring nucleus interior	Crater scan	
I+110 s to I+67 s	70	Ejecta monitoring post-impact coma	Exposures every 10% of time from impact	

(Continued on next page)

TABLE III
(Continued)

Time ^a	Pixel Scale (m)	Scientific goals	Data description	Comments
I+180 s to I+490 s	68–37	Nucleus interior post-impact coma	Full nucleus scan including off edges for inner coma	3 full resolution at edges and nucleus center
I+497 s to SM–142 s	37–21	Nucleus interior	Scan of central 1/4 nucleus	
SM–130 s to SM–110 s	18	Post-impact coma	Three coma observations	
SM–98 s to SM–26 s	16–9	Nucleus interior	Exposures every 2.88 s plus scan 3 × crater diameter	Last partial nucleus scan
Shield mode				
SM–23 s to SM	8–7	Nucleus interior	Exposures every 2.88 s	Highest resolution before shield mode
SM+3 s to SM+1 m	7	Post-impact coma	Long (7–14 s) exposures for faint molecules	Significant smear at any exposure
Look back				
SM+33 m to SM+62 m	200–400	Nucleus interior post-impact coma	Scan across nucleus plus 3 different coma positions	Repeated 3 times in this time interval
SM+2 h to SM+6 h	>700	Post-impact coma	3 different coma positions taken every 2 h	Full resolution
SM+12 h to SM+60 h	>4300	Post-impact coma	3 different coma positions taken every 6 h	Full resolution

^aI: Impact; SM: Shield mode.

comet from 1–5 μm prior to impact at higher spatial resolution and over longer time scales than ever before. In addition, we will use the HRI-IR spectrometer to monitor our impact experiment obtaining data on ejecta over time, and changes in dust and gas emission. Finally, by observing the crater and its surrounding ejecta deposits, we hope to directly observe the interior of the comet. In the above discussions, we largely speculate on what we might observe. The only certain outcome, should the Deep Impact successfully complete its mission, is that our current understanding of comets will undoubtedly change.

TABLE IV
The predicted HRI-IR spectrometer mean signal levels and SNRs^a.

Wavelength (μm)	Mean nucleus DN	Mean nucleus SNR	Mean coma DN	Mean coma SNR
1.2	49	27	2	1
2	199	55	5	2
2.8 (300 K, filt)	700	102		
3.6 (300 K, filt)	5500	287		
4.6 (300 K, filt)	20	17		
2.8 (200 K, no filt)	115	42	2	1
3.6 (200 K, no filt)	92	37	2	1
4.6 (200 K, no filt)	199	55	3	1

^aFilt: behind the anti-saturation filter; no filter: outside the filter, see text.

Acknowledgments

This research is supported by the Deep Impact Discovery mission, Science Mission Directorate, NASA Headquarters. The Deep Impact science team is managed by Dr. Michael A'Hearn through the University of Maryland. The authors are particularly indebted to the hard work and dedication of the HRI-IR spectrometer engineering team led by Don Hampton (Ball Aerospace and Technology Corporation) and Dennis Wellnitz (University of Maryland). Reviews by J. Crovisier and an anonymous reviewer are greatly appreciated and helped clarify this manuscript.

References

- Abell, P. A., *et al.*: 2003, *LunarPlanet. Sci. Conf.* **34**, abstract 1253.
 Abell, P. A., *et al.*: 2005, *Icarus*, submitted.
 A'Hearn, M. F., Millis, R. L., Schleicher, D. G., Osip, D. J., and Birch, P. V.: 1995, *Icarus* **118**, 223.
 Barucci, M. A., de Bergh, C., Cuby, J.-G., Le Bras, A., Schmitt, B., and Romon, J.: 2000, *Astron. Astrophys.* **357**, L53.
 Barucci, M. A., Cruikshank, D. P., Mottola, S., and Lazzarin, M.: 2002, in Bottke, *et al.* (eds.), *Asteroids III*, University of Arizona Press, Tucson, p. 273.
 Barucci, M. A., Doressoundiran, A., and Cruikshank, D. P.: 2005, in Festou, M., Keller, H. U., and Weaver, H. A. (eds.), *Comets II*, University of Arizona Press, Tucson, in press.
 Belton, M. J., *et al.*: 2005, *Space Sci. Rev.*, this volume.
 Bockelée-Morvan, D., *et al.*: 2000, *Astron. Astrophys.* **353**, 1101.
 Bockelée-Morvan, D., Brooke, T. Y., and Crovisier, J.: 1995, *Icarus* **116**, 18.
 Brin, G. D., and Mendis, D. A.: 1979, *Astrophys. J.* **229**, 402.
 Brown, M. E. and Koresko, C. C.: 1998, *Astrophys. J. Lett.* **505**, L65.
 Brown, R. H., Cruikshank, D. P., and Pendleton, Y.: 1999, *Astrophys. J.* **519**, 101.

- Brown, M. E.: 2000, *Astron. J.* **119**, 977.
- Brownlee, D. E., *et al.*: 2004, *Science* **304**, 1764.
- Burns, R. G.: 1993, *Mineralogical Applications of Crystal Field Theory*, Cambridge University Press, New York, p 551.
- Campins, H., Licandro, J., Guerra, J., Chamberlain, M., and Pantin, E.: 2003, *AAS/DPS* **35**, abstract 47.02.
- Clark, R. N.: 1981, *J. Geophys. Res.* **86**, 3087.
- Cloutis, E. A.: 1990, *Science* **245**, 165.
- Colangeli, L.: 1999, *Astron. Astrophys.* **343**, L87.
- Coradini, L., *et al.*: 1998, *Plant. Space Sci.* **46**, 1291.
- Combes, M., *et al.*: 1988, *Icarus* **76**, 404.
- Crovisier, J. and Encrenaz, T.: 1983, *Astron. Astrophys.* **126**, 170.
- Crovisier, J., *et al.*: 1997, *Science* **275**, 1904.
- Crovisier, J., *et al.*: 1999a, *ESA-SP* **427**, 137.
- Crovisier, J., *et al.*: 1999b, *ESA-SP* **427**, 161.
- Cruikshank, D. P., *et al.*: 1998, *Icarus* **135**, 389.
- Delahodde, C., Hainaut, O. R., Romin-Martin, J., and Lamy, P. L.: 2002, *Astr. Comets Met. Confer.*, abstract 20.08.
- Dotto, E., Barucci, M. A., Leyrat, C., Romon, J., de Bergh, C., and Licandro, J.: 2003, *Icarus* **164**, 122.
- Ernst, C. and Schultz, P.: 2003, *Lunar Planet. Sci. Conf.* **34**, abstract 2020.
- Ernst, C. and Schultz, P.: 2004, *Lunar Planet. Sci. Conf.* **35**, abstract 1721.
- Groussin, O. and Lamy, P.: 2003, *Astron. Astrophys.* **412**, 879.
- Groussin, O., Lamy, P., and Jorda, L.: 2004a, *Astron. Astrophys.* **413**, 1163.
- Groussin, O., *et al.*: 2004b, *COSPAR* **35**, abstract B1.1 002204.
- Groussin, O., Lamy, P., Jorda, L., and Toth, I.: 2004c, *Astron. Astrophys.* **419**, 375.
- Gruen, E., Schwehm, G., Massonne, L., Fertig, J., and Graser, U.: 1985, *Lunar Planet. Sci. Conf.* **16**, 28.
- Hainaut, O. R., *et al.*: 2000, *Astron. Astrophys.* **356**, 1076.
- Harker, D. E., Wooden, D. H., Woodward, C. E., and Lisse, C. M.: 2002, *Astrophys. J.* **580**, 579.
- Hampton, D., *et al.*: 2005, *Space Sci. Rev.*, this volume.
- Hunt, G. R.: 1979, *Geophysiscs* **44**, 1974.
- Hunt, G. R. and Ashley, R. P.: 1979, *Econ Geol* **74**, 1613.
- Jessberger, E. K., Christoforidis, A., and Kissel, J.: 1988, *Nature* **332**, 691.
- Jewitt, D. C.: 1991, in Newburn, R. L., Neugebauer, M., and Rahe J. H. (eds.), *Comets in the Post-Halley Era*, Kluwer Academic Publishers, Dordrecht, Holland, p. 1043.
- Jewitt, D. C. and Luu, J. X.: 2001, *Astrophys. J.* **122**, 2099.
- Johnson, R. E., Cooper, J. F., Lanzerotti, L. J., and Strazzulla, G.: 1987, *Astron. Astrophys.* **187**, 889.
- Kern, S. D., McCarthy, D. W., Buie, M. W., Brown, R. H., Campins, H., and Rieke, M.: 2000, *Astrophys. J.* **542**, L155.
- Kissel, J., Krueger, F. R., Silen, J., and Clark, B. C.: 2004, *Science* **304**, 1774.
- Klaasen, K. P., Carcich, B. Carcich, G., and Grayzeck, E. J.: 2005, *Space Sci. Rev.*, this volume.
- Krasnopolsky, V. A., *et al.*: 1986, *Nature* **321**, 269.
- Lamy, P. L., Gruen, E., and Perrin, J. M.: 1987, *Astron. Astrophys.* **187**, 767.
- Lamy, P. L., Malburet, P., Llebaria, A., and Koutchmy, S.: 1989, *Astron. Astrophys.* **222**, 316.
- Lamy, P., Toth, I., Jorda, L., Groussin, O., A'Hearn, M. F., and Weaver, H. A.: 2002, *Icarus* **156**, 442.
- Lellouch, E., *et al.*: 1998, *Astron. Astrophys.* **339**, L9.
- Levison, H. F. and Duncan, M. J.: 2001, *Astrophys. J.* **121**, 2253.
- Licandro, J., Oliva, E., and Di Martino, M.: 2001, *Astron. Astrophys.* **373**, L29.
- Licandro, J., *et al.*: 2002, *Earth Moon Planets* **90**, 495.

- Licandro, J., Campins, H., Hergenrother, C., and Lara, L. M.: 2003, *Astron. Astrophys.* **398**, L45.
- Lisse, C. M., *et al.*: 1998, *Astrophys. J.* **496**, 971.
- Lisse, C. M., Fernandez, Y. R., and Biesecker, D. A.: 2002, *DPS* **34**, abstract 12.06.
- Lisse, C. M., A'Hearn, M. F., Farnham, T., Groussin, O., Meech, K. J., and Fink, U.: 2005, *Space Sci. Rev.*, this volume.
- Luu, J. X.: 1993, *Icarus* **104**, 138.
- Luu, J. X. and Jewitt, D. C.: 1996, *Astrophys. J.* **112**, 2310.
- Luu, J. X. and Jewitt, D. C.: 1998, *Astrophys. J. Lett.* **494**, L117.
- Luu, J. X., Jewitt, D. C., and Trujillo, C.: 2000, *Astrophys. J.* **531**, L151.
- McDonnell, J. A. M., Lamy, P. L., and Pankiewicz, G. S.: 1991, in Newburn, R. L., Neugebauer, M., and Rahe J. H. (eds.), *Comets in the Post-Halley Era*, Kluwer Academic Publishers, Dordrecht, pp. 1043.
- Moroz, L. V., Arnold, G., Korochantsev, A. V., and Wasch, R.: 1998, *Icarus* **134**, 253.
- Moroz, L. V., *et al.*: 2004, *Icarus* **170**, 214.
- Mumma, M. J., *et al.*: 2001, *Astrophys. J.* **546**, 1183.
- Nelson, R. M., Rayman, M. D., and Weaver, H. A.: 2004, *Icarus* **167**, 1.
- Nemtchinov, I. V., Shuvalov, V. V., Artemieva, N. A., Kosarev, I. B., and Trubetskaya, I. A.: 1999, *Int. J. Impact Eng.* **23**, 651.
- Quirico, E., *et al.*: 1999, *Icarus* **139**, 159.
- Rayner, J. T., *et al.*: 2003, *Astron. Soc. Pac.* **805**, 362.
- Rothman, L. S., *et al.*: 2003, *J. Quant. Spect. Rad. Trans.* **82**, 5–44 (<http://www.hitran.com>).
- Soderblom, L. A., *et al.*: 2004a, *Icarus* **167**, 4.
- Soderblom, L. A., *et al.*: 2004b, *Icarus* **167**, 100.
- Schultz, P.: 1996, *J. Geophys. Res.* **101**(E9), 21117.
- Schultz, P. and Ernst, C.: 2005, *Space Sci. Rev.*, this volume.
- Sugita, S., Schultz, P. H., and Hasegawa, S.: 2003, *J. Geophys. Res.* **108**(E6), 5140.
- Thomas, P., *et al.*: 2005, *Space Sci. Rev.*, this volume.